



Energy analysis of structural changes in pianos

Antoine Chaigne, Juliette Chabassier, Marc Duruflé

► To cite this version:

Antoine Chaigne, Juliette Chabassier, Marc Duruflé. Energy analysis of structural changes in pianos. Vienna Talk on Music Acoustics, Sep 2015, Vienna, Austria. hal-01296947

HAL Id: hal-01296947

<https://hal.science/hal-01296947>

Submitted on 4 Apr 2016

HAL is a multi-disciplinary open access archive for the deposit and dissemination of scientific research documents, whether they are published or not. The documents may come from teaching and research institutions in France or abroad, or from public or private research centers.

L'archive ouverte pluridisciplinaire **HAL**, est destinée au dépôt et à la diffusion de documents scientifiques de niveau recherche, publiés ou non, émanant des établissements d'enseignement et de recherche français ou étrangers, des laboratoires publics ou privés.

ENERGY ANALYSIS OF STRUCTURAL CHANGES IN PIANOS

Antoine Chaigne

Institute of Music Acoustics
University of Music and Performing Arts
Vienna, Austria
chaigne@mdw.ac.at

Juliette Chabassier; Marc Duruflé

Magique 3D Team
Inria Bordeaux Sud Ouest, France
juliette.chabassier@inria.fr
marc.duruflé@inria.fr

ABSTRACT

The leading idea of this theoretical paper is to examine the effects of structural changes in the piano on the basis of energetic quantities relative to its constitutive parts. These energies are global quantities which characterize the intrinsic properties of the instrument, irrespective of the observation point. The evolution of the various energy terms with time are calculated with a help of a recent piano model which couples together the hammer, the nonlinear strings, the soundboard and the acoustic space [1]. Some parameters, which play a major role in the history of the piano are particularly examined: string tension and diameter, soundboard thickness and rigidity, hammer mass and velocity. The results show that direct links can be established between the energetic quantities and the tonal properties of the piano sounds, in terms of temporal envelope and spectral content. They also shed useful light on the energy exchange between the constitutive parts of the instrument, and on its acoustical efficiency. This study is intended to have potential applications as a theoretical guideline for piano making, restoration and reproduction of historic instruments.

1. INTRODUCTION

This paper reports the first part of a study, whose aim is to establish links between physical construction parameters and sound properties in pianos. The leading idea of the project is to investigate to what extent the future sound qualities of a piano can be predicted by a set of geometrical and material data related to its different constitutive parts and on their assembly conditions. The results of this study could be used for the initial sketch in the design of a new instrument, and for prediction of the effects of structural changes in piano restoration. It should also be useful for a better understanding of the evolution of sound quality in piano history.

Twenty years ago, a systematic exploration of piano parameters was done by the author, though this study was restricted to the string-hammer system only [2]. More recently, French developed a theoretical framework for describing the effects of structural modifications in the soundboard-soundbox system in guitars [3]. Here, the study is based on a recent piano model developed by Chabassier which couples together the nonlinear strings, the hammer, the vibrating soundboard and the acoustic field [4, 1].

This piano simulation model is discretized in time and space and yields, as a result, the time history of a number of physical quantities: sound pressure, soundboard vibrations, strings and hammer motion, energetic quantities. It allows the variation of one single geometrical or material parameter at a time, independently of the others. The model is based on a *dynamical* (and not *static*) behavior of the instrument. This enables us to investigate the effects of structural changes that would often

be impossible to achieve in the reality. However, in its present state, the model does not have the capacity of reproducing all the necessary fine adjustments made in the development of a real piano. In this respect, it can be viewed as a complementary tool of the usual piano design procedure in a workshop. In this paper, focus is put on energetic vibratory and acoustic quantities. These quantities are obtained through spatial integration of the dynamic variables in each domain of the constitutive elements of the piano. As a result, we obtain functions of time, only. The advantage of examining such quantities is that it yields a *global* assessment of the instrument as a source, irrespective of the listening (or recording) point. They also shed useful light on the energy exchanges due to the coupling between all parts of the instruments.

The paper starts with a summary of the model, which has already been described elsewhere extensively [4, 1]. Attention is paid to energetic quantities which are thereafter thoroughly discussed. The results are given for one single note (Steinway D, C♯5, Nr 53, fundamental $f_1=555$ Hz). The study is concentrated on some selected parameters of strings (tension at rest, diameter), hammer (mass, striking velocity) and soundboard (thickness, elasticity). These parameters are known to have important effects on piano tones, and have evolved significantly in the history of piano making [5, 6]. However, as far as we are aware, they have not been yet the subject of any systematic theoretical study in the past, essentially because of the absence of a reliable model where the main elements of the piano are coupled together.

2. MODEL AND METHOD

2.1. Model

In its present state, the piano model starts with the impact of a hammer of mass M_H with initial velocity V_H on a string (or on a set of 2 to 3 strings, depending on the note). The complex mechanism that transmits the action of the player from key to hammer is ignored. The strings vibrate both transversely and longitudinally, these two regimes being non-linearly coupled. Transverse and longitudinal string forces are transmitted to the soundboard at the bridge. The soundboard is modeled as a dissipative orthotropic Reissner-Mindlin plate. The ribs and bridges are modeled as local heterogeneities in thickness and rigidity (see Figure 1). The soundboard radiates sound in a closed box surrounding the instrument (see Figure 2). The other parts of the instrument are assumed to be rigid. The box is delimited by absorbing regions (Perfectly Matched Layers, or PML) so that no outgoing waves return back to the piano.

The equations of the model are discretized in time and space. The stability criteria of the numerical formulation are based on energy conservation. The input set of parameters of the simu-

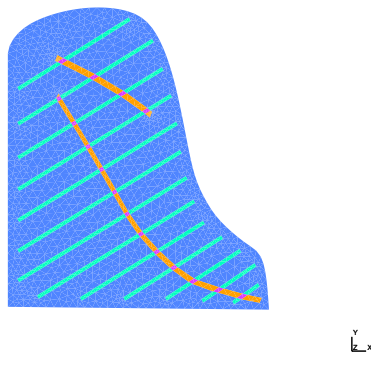


Figure 1: Model of a Grotrian-Steinweg soundboard. The ribs and bridge are modeled as local heterogeneities in thickness and rigidity.

lations is composed of the geometrical and material data of the constitutive elements of the piano: hammer, strings, soundboard and air (see Table 1). The main output files are physical functions of time (string displacement, hammer force, soundboard acceleration, sound pressure, energetic quantities) and most of them can be heard after appropriate digital-to-analog conversion, which allows an auditory evaluation of the structural modifications. Soundboard's eigenfrequencies and mode shapes also are available. In total, the numerical model requires heavy calculations. As an example, the order of magnitude for the number of degrees of freedom (dof) is 1.4×10^5 for the soundboard, and 2.3×10^7 for the acoustic space.

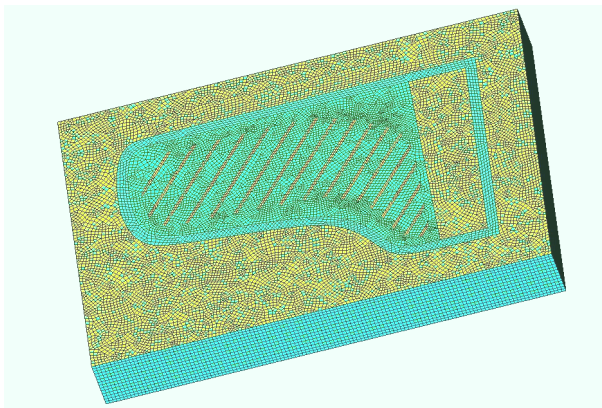


Figure 2: Closed box delimiting the acoustic field radiated by a Steinway D piano (seen from bottom). The box is delimited by absorbing regions (PML).

The equations of the model and their numerical treatment were presented in detail in previous papers, and will not be developed further here [4, 1]. However, since the results and the discussion that follows mainly refer to energetic quantities, these expressions are now briefly reviewed.

2.2. Energetic quantities

At the origin of time, the initial energy imparted to the piano is the kinetic energy of the hammer:

$$\mathcal{E}_0 = \frac{1}{2} M_H V_H^2. \quad (1)$$

The energy of the constitutive elements of the piano are obtained through spatial integration over their respective domains. As a result, we obtain the evolution with time of a scalar quantity that fully characterizes each element, irrespective of the observation point. For simplicity, the dissipation terms are ignored in the energetic quantities given in this section, although these terms are present in the simulations. The expression of the various sources of losses in the piano model are reviewed in the Appendix (see Section 6).

2.2.1. String energy

The energy $\mathcal{E}_s(t)$ of a non-dissipative nonlinear string s is given by:

$$\mathcal{E}_s(t) = \mathcal{E}_{s,kin}(t) + \mathcal{E}_{s,pot}(t) \quad (2)$$

where the kinetic energy is:

$$\begin{aligned} \mathcal{E}_{s,kin}(t) &= \frac{\rho A}{2} \int_0^L \left(\frac{\partial u_s}{\partial t} \right)^2 dx \\ &+ \frac{\rho A}{2} \int_0^L \left(\frac{\partial v_s}{\partial t} \right)^2 dx + \frac{\rho I}{2} \int_0^L \left(\frac{\partial \varphi_s}{\partial t} \right)^2 dx, \end{aligned} \quad (3)$$

and the elastic potential energy [7]:

$$\begin{aligned} \mathcal{E}_{s,pot}(t) &= \frac{T_0}{2} \int_0^L \left(\frac{\partial u_s}{\partial x} \right)^2 dx + \frac{EA}{2} \int_0^L \left(\frac{\partial v_s}{\partial x} \right)^2 dx \\ &+ \frac{EI}{2} \int_0^L \left(\frac{\partial \varphi_s}{\partial x} \right)^2 dx + \frac{AG\kappa}{2} \int_0^L \left(\frac{\partial u_s}{\partial x} - \varphi_s \right)^2 dx \\ &+ (EA - T_0) \int_0^L \left[\frac{1}{2} \left(\frac{\partial u_s}{\partial x} \right)^2 + \left(1 + \frac{\partial v_s}{\partial x} \right) - \sqrt{\left(\frac{\partial u_s}{\partial x} \right)^2 + \left(1 + \frac{\partial v_s}{\partial x} \right)^2} \right] dx, \end{aligned} \quad (4)$$

In these expressions, u_s is the vertical transverse displacement, v_s the longitudinal displacement and φ_s the rotation of the cross-sections. The string is defined by the following parameters: length L , density ρ , cross-sectional area A , flexural inertia I , tension at rest T_0 , Young's modulus E , torsional modulus G , and shear correction factor κ (Timoshenko's parameter). Examples of parameters are given in Table 1 for the note C♯5. In the absence of internal dissipation, and for no coupling with air and soundboard, $\mathcal{E}_s(t)$ is constant after the hammer has left the string, and is then equal to the total energy imparted by the striking hammer.

2.2.2. Hammer energy

The hammer strikes the string at position x_H . As a result, the hammer force F_H imparted to the string is described by:

$$F_H(t) = K_H \Phi(\langle u_s \rangle(t) - \xi(t)). \quad (5)$$

where K_H is a stiffness coefficient, and Φ is a standard nonlinear power function of the distance d between the hammer position ξ and the position of the string $\langle u_s \rangle$ averaged over the length of the hammer-string contact [8, 9]. The force F_H is limited in time to the instants where the hammer is in contact with the string i.e., when the string-hammer distance is smaller than the reference distance obtained when the string is just touching the undeformed felt, at the origin of time. Defining then further the function $\Psi(d) = \int_d^{+\infty} \Phi(s) ds$, one can

show that the energy of the hammer interacting with the string s is written [4]:

$$\mathcal{E}_H(t) = K_H \Psi(\langle u_s \rangle(t) - \xi(t)) + \frac{M_H}{2} \left(\frac{d\xi}{dt}(t) \right)^2. \quad (6)$$

This expression again is valid for a non-dissipative hammer only. In the model, a dissipative term is added to the stiffness term in Eq. (5) to account for the relaxation of the felt (see Appendix).

2.2.3. Soundboard energy

Similarly to the strings, the energy $\mathcal{E}_p(t)$ of the soundboard is:

$$\mathcal{E}_p(t) = \mathcal{E}_{p,kin}(t) + \mathcal{E}_{p,pot}(t) \quad (7)$$

where the kinetic energy is:

$$\begin{aligned} \mathcal{E}_{p,kin}(t) &= \iint_{\omega} \rho_p \delta \left(\frac{\partial u_p}{\partial t} \right)^2 dx dy + \\ &\quad \iint_{\omega} \rho_p \frac{\delta^3}{12} \left| \frac{\partial \underline{\theta}_p}{\partial t} \right|^2 dx dy, \end{aligned} \quad (8)$$

and the elastic potential energy:

$$\begin{aligned} \mathcal{E}_{p,pot}(t) &= \iint_{\omega} \frac{\delta^3}{12} \mathbf{C} \underline{\varepsilon}(\underline{\theta}_p) : \underline{\varepsilon}(\underline{\theta}_p) dx dy + \\ &\quad \iint_{\omega} \delta \kappa^2 \cdot \underline{G} |\nabla u_p + \underline{\theta}_p|^2 dx dy. \end{aligned} \quad (9)$$

Here, ρ_p is the density of the soundboard, and δ its thickness. Both quantities can be space-dependent, which is necessary for representing bridges and ribs. u_p is the transverse displacement, $\underline{\theta}_p$ is the local rotation vector, and $\underline{\varepsilon}$ is the linearized strain tensor. \mathbf{C} is an orthotropic elasticity tensor which, again, depends on space. This tensor can then also account for the presence of bridge and ribs. It is easily possible to modify this tensor in order to change the elastic properties of the soundboard (consecutive to a pre-stress due to the crown, for example) without changing its mass. In the simulations, additional terms account for the dissipation inside the material.

2.2.4. Acoustic energy

Finally, the acoustic energy $\mathcal{E}_a(t)$ radiated by the instrument is given by:

$$\begin{aligned} \mathcal{E}_a(t) &= \iint_{\Omega} \frac{\rho_a}{2} |\underline{v}_a|^2 dx dy dz + \\ &\quad \iiint_{\Omega} \frac{\mu_a}{2} p^2 dx dy dz, \end{aligned} \quad (10)$$

where ρ_a is the air density, and μ_a its compressibility. \underline{v}_a is the acoustic velocity and p is the sound pressure.

All energetic quantities (2)-(4) and (5)-(10) yield valuable insight into the time history of the transmission of energy from string to soundboard, and, in turn, from the soundboard to the acoustic space, over the duration of a piano tone. Derivations of these quantities versus time allow further to describe the phenomena in terms of power. From the ratio between soundboard and total energy (resp. between acoustic and total energy), we gain useful information on the vibrational (resp. acoustical) efficiency of the instrument, and on the variations of these efficiencies consecutive to structural modifications.

2.3. Selection of notes and parameters

The program is able to simulate the 88 notes of a modern grand piano. Amongst these, particular notes were simulated in the past and compared for validation to measurements on a Steinway D grand piano: D \sharp 1, C2, F3, C4, C \sharp 5, G6 (see [1]). Other measurements on a large variety of pianos are currently under way. The objective of the present paper is not to reproduce one given instrument, but rather to exhibit the main principles of energy analysis. Therefore, the effects of structural changes are analyzed below for one single note (C \sharp 5), and for a simple soundboard of constant thickness. Refined modifications related to ribs and bridges are left for a future report. The investigated modifications reported here are inspired by the main tendencies observed in the history of piano making. In addition, the change of parameters were selected to be made easily in the present version of the simulation program.

- The variation of string tension is a key feature observed in the history piano making. In the past, low string tension was imposed because it was entirely withstood by the soundboard. With the evolution of more powerful and louder instruments, the strings of modern pianos are now fixed on cast iron frames, thus allowing higher tension. In order to keep the same pitch in the present study, the diameter of the strings is modified so that the transverse velocity of the waves is kept constant. The inertia coefficient is modified accordingly.
- Another currently observed evolution is related to the mass of the hammers, which generally tend to increase throughout the history of piano making. The initial velocity of the hammer is also used as a varying parameter, for comparison.
- The thickness δ of the soundboard is an essential parameter which influences both its mass and rigidity. As a consequence, it has an extreme influence on the transmission of energy from strings to soundboard and from soundboard to air. A fortunate aspect of the present piano model lies in the possibility of modifying this parameter over a wide range of values, without considering the consequences in terms of soundboard weakness and risks of breaking. Since the prime purpose here is to observe the physical consequences of structural modifications, the range of thickness goes here far beyond those observed on real pianos.
- In our model, the rigidity of the soundboard can also be modified, independently from its mass and structure, just by modifying the elastic constants. This might correspond to *virtual* materials, but also to the effect of crown in real pianos. It is generally admitted that increasing the soundboard rigidity contributes to produce a louder sound, and thus we want to verify this point and quantify it in terms of physical quantities.

3. RESULTS AND DISCUSSION

The numerical simulations reported below are made for a “complete” piano, where the 3 strings (note C \sharp 5) are coupled to a Steinway D grand piano soundboard (without ribs and bridges), this soundboard being coupled to the acoustic field. The other parts of the piano (case, keybed, frame) are supposed to be rigid. The sound duration is 1 s. A list of the main parameters for the note C \sharp 5 is given in Table 1.

3.1. Variations of string tension and diameter

Figure 3 shows the time evolution of the total energy of the piano, for three different tensions of the strings. All other parameters remain unchanged, except the diameter of the string which varies in proportion to the square root of the tension in order to keep the same pitch. All three curves start with the

| Hammer | |
|-------------------------------------|-----------------------------------|
| Mass M_H | 7.9 g |
| Velocity V_H | 3 m/s |
| Stiffness K_H | $2.8 \cdot 10^{10}$ SI-units |
| Striking position x_H | 0.039 m |
| String | |
| Length $L (\times 3)$ | 0.3255 m |
| Cross-sectional area of strings A | $6.66 \cdot 10^{-7} \text{ m}^2$ |
| Tension T_0 | 687 N |
| Density ρ | 7850 kg/m^3 |
| Young's modulus E | $2.0 \cdot 10^{11} \text{ N/m}^2$ |
| Torsional modulus G | $8.0 \cdot 10^{10} \text{ N/m}^2$ |
| Shear correction factor κ | 0.85 |
| Moment of inertia I | $3.5 \cdot 10^{-14} \text{ m}^4$ |
| Soundboard (Spruce) | |
| Density ρ_p | 380 kg/m^3 |
| Thickness δ | 10 mm |
| Longitudinal modulus E_L | $11.0 \cdot 10^9 \text{ N/m}^2$ |
| Transverse modulus E_T | $650 \cdot 10^6 \text{ N/m}^2$ |

Table 1: Main parameters used for the reference note C \sharp 5.

same initial energy ($\mathcal{E}_0 = 0.0355 \text{ J}$) imparted by the hammer. The middle curve corresponds to the nominal tension $T_0 = 687 \text{ N}$, while the upper and the lower curves correspond to $T_0/2$ and $3T_0/2$, respectively. The three curves show a more or less rapid decrease up to 0.1 s, and then stabilize. However, the initial decrease is much more pronounced for the nominal and high tension than for the low tension. For low tension, the energy is maintained longer confined in the strings.

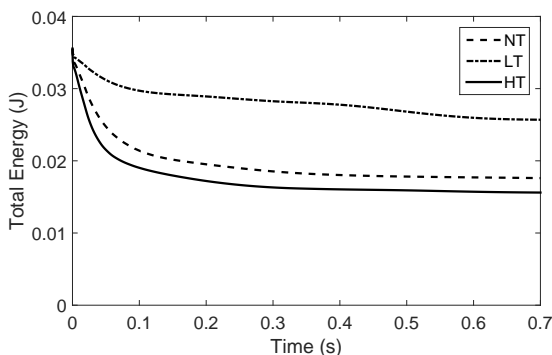


Figure 3: Time evolution of the total energy of the piano for three different tensions of the strings. Note C \sharp 5. Upper curve: $T_0/2$ (Low Tension); middle curve: T_0 (Normal Tension); lower curve: $3T_0/2$ (High Tension).

This result is a direct consequence of the impedance matching at the bridge. As seen in Figure 4, the maximum of the relative soundboard energy ratio follows the same order as the tensions, which shows that more string energy is transmitted to the soundboard when the tension is higher. Another significant feature of this figure is that the soundboard energy is damped more rapidly for high string tension than for low tension, which means that the structural and radiation losses are higher in relative value. This can be explained by the fact that both the internal viscoelastic losses in the soundboard and the radiated energy vary as the square of the velocity (see Appendix).

Finally, it is seen in Figure 4 that the relative acoustic energy radiated by the piano follows the same time evolution as the soundboard, for each tension. This is due to the fact that the

soundboard is identical in the three cases.

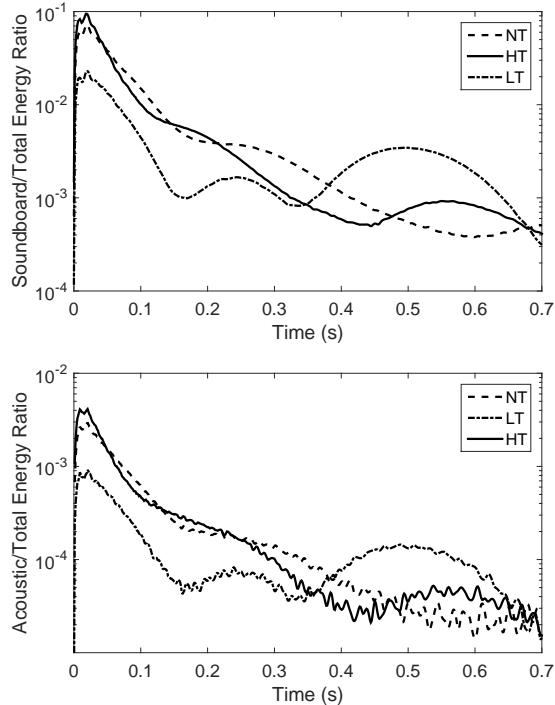


Figure 4: Time evolution of the relative soundboard energy (top) and acoustic energy (bottom) for three different tensions of the strings. High tension: solid line; normal tension: dashed line; low tension: dash-dotted line. Note C \sharp 5.

Simulations of the sound pressure at a given fixed point in space ($z=38 \text{ cm}$ above the soundboard) are coherent with these results (see Figure 5). For this figure, as for the following ones, the origin of the axes ($x = 0, y = 0, z = 0$) is situated on the lowest left corner of the soundboard (bass range). As expected, the maximum of the pressure increase with strings' tension, and the decay time is longer for low tension. This result is of prime importance, since the pressure is the acoustic variable that we hear. However, from the point of view of piano manufacturing, the results based on energy considerations presented in Figure 4 have a more general meaning, since they are valid for the instrument (the sound source) as a whole.

3.2. Variations of soundboard thickness and rigidity

In this section, the energetic quantities and sound pressure envelopes are compared for three different soundboards: the reference soundboard (TSB) whose parameters are listed in Table 1, a thin soundboard (VTSB) of thickness $\delta = 7 \text{ mm}$, and a rigid soundboard (RIG) with the reference thickness, but where all elasticity moduli are multiplied by a factor of 2.

Figure 6 illustrates the effects of thickness and rigidity changes on the eigenfrequencies of the three soundboards. In each case, the simulations are made taking the 800 first modes of the soundboard into account. The theory predicts that the asymptotic modal density is nearly inversely proportional to the thickness and to the square root of the elasticity moduli [10]. This is coherent with the results obtained here, where the maximum frequency of the modes for the thin soundboard is 3413 Hz, i.e. 0.8 times the 800th eigenfrequency of the reference soundboard (4229 Hz). Similarly, the 800th eigenfrequency of the rigid soundboard is 5981 Hz, which is 1.4 times higher than the

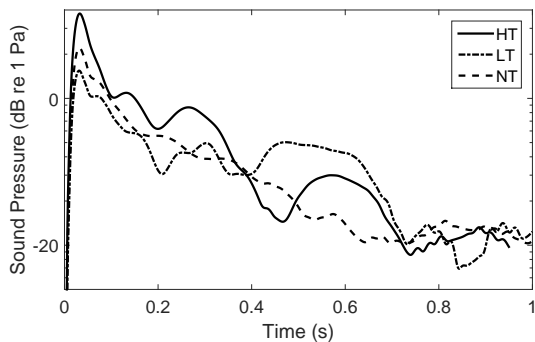


Figure 5: Time envelope of the sound pressure at a point of coordinates ($x=0.85$; $y=1.46$; $z=0.38$) m for three different strings' tensions. The x -axis is parallel to the keys, the y -axis is perpendicular to it in the soundboard plane, and the z -axis is perpendicular to the soundboard. The origin of the axes is at the lowest left corner of the soundboard (bass side). High tension ($3T_0/2$): solid line; normal tension (T_0): dashed line; low tension ($T_0/2$): dash-dotted line.

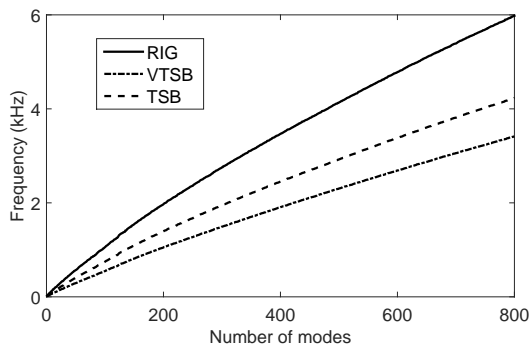


Figure 6: Soundboard eigenfrequencies in three different cases: Reference (TSB, dashed line), thin soundboard (VTSB, dash-dotted line), rigid soundboard (RIG, solid line).

reference soundboard. Before moving to other considerations, let us point out that these modifications of the eigenspectrum are responsible for changes in tone color since most of the soundboard modes are excited during the transients of piano tones.

Figure 7 shows the time evolution of energy ratios for the three soundboards during the initial part of a piano tone (0.4 s). The thin soundboard (VTSB) has the highest soundboard/total energy ratio, and its maximum is reached the most rapidly (after 14 ms). This is due to the fact that the velocity profile of this soundboard is higher than for the reference one. However, this ratio also shows the most rapid decrease, again because the losses in the soundboard increase with the square of the velocity (see Appendix). The rigid soundboard (RIG) also has more energy than the reference one (TSB), due this time to an increase in potential elastic energy (see Eq. 9), and its decay times lies between the two others. Examining now the acoustic/total energy ratios shows substantial differences: here the rigid soundboard generates almost the same acoustic energy as the thin one, but this energy lasts significantly longer. As shown in the bottom of the figure, this result is due to a more efficient structural-acoustic coupling for the rigid soundboard than for the others, and less rapid losses. This is in accordance with the general theory of vibroacoustics which predicts that the

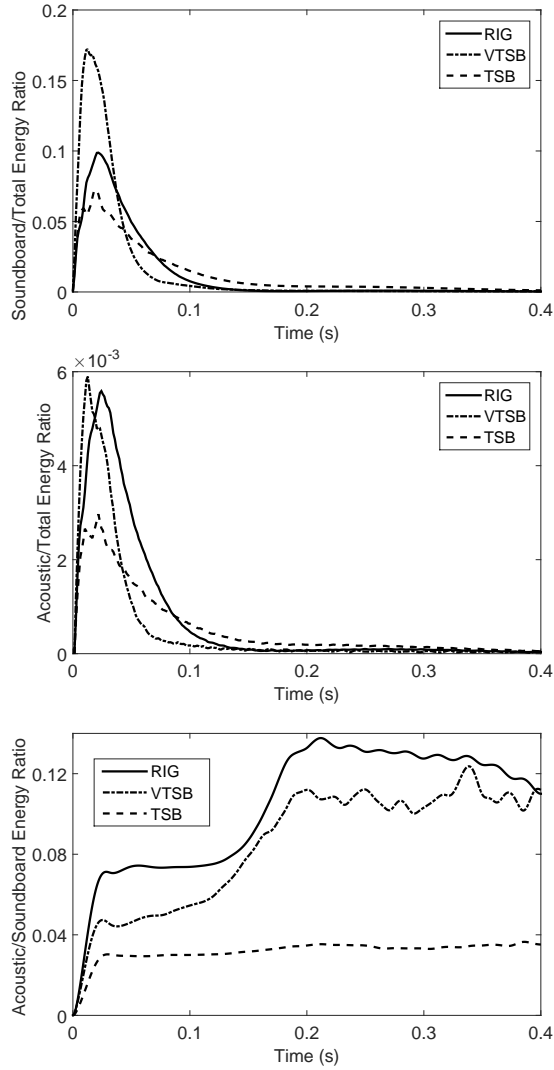


Figure 7: (Top) soundboard energy vs total energy. (Middle) radiation efficiency of the instrument: Ratio acoustic energy vs total energy. (Bottom) Vibroacoustic coupling: ratio acoustic energy vs soundboard energy. Time evolution. TSB (dashed line): reference soundboard; VTSB (dash-dotted line): thin soundboard; RIG (solid line): rigid soundboard.

acoustical efficiency of a plate increases with the stiffness [11]. In this presented case, the gain in acoustical efficiency due to stiffness exceeds the decrease due to reduction of the mean velocity, compared to the thin soundboard. In piano making, it is well-known that imposing an initial dome shape (or crown) to the soundboard is a good way to enhance the radiation of the instrument through increase of stiffness, without change of mass. Attaching ribs to the soundboard produces similar effects, though with a slight increase of mass.

The results based on energy considerations for the source are confirmed on the time envelope of the sound pressure at the point of coordinates ($x=0.85$; $y=1.46$; $z=0.38$) m (see Figure 8). For this particular selected point, the rigid plate yields the louder sound. Although it decreases faster than the reference sound during the initial transient, it stays in average louder for the entire duration of the tone. The sound pressure simulated with the thin soundboard also starts with a louder sound than the reference one but, in this latter case, it decays significantly

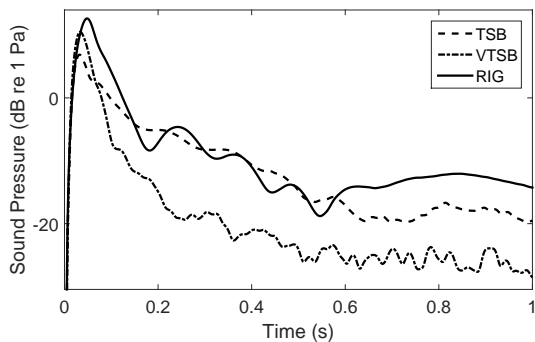


Figure 8: Time envelope of the sound pressure at the point of coordinates ($x=0.85$; $y=1.46$; $z=0.38$) m for three soundboards. Solid line: rigid soundboard (RIG); dashed line: reference soundboard (TSB); dash-dotted line: thin soundboard (VTSB).

faster.

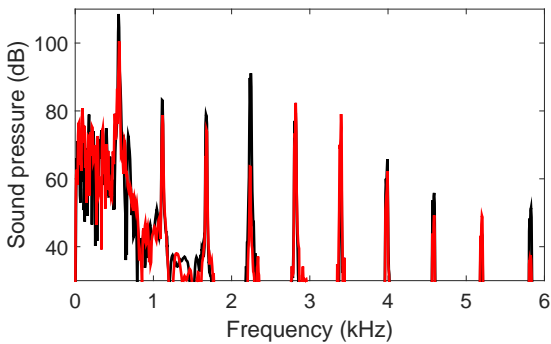


Figure 9: Spectra of the sound pressure simulated at the point of coordinates ($x=0.85$; $y=1.46$; $z=0.38$) m. Initial transient (duration 0.4 s). RIG (black) and VTSB (red) soundboards.

Modifying the properties of the soundboard has additional consequences on the sound spectrum. Figure 9 shows a comparison between the spectra calculated at the same point in space for the rigid and thin soundboards, respectively. In accordance with the eigenfrequencies displayed in Fig. 6, we can see on the lower part of the initial transient spectra that the excited frequency band of the soundboard modes is broader for the rigid soundboard than for the thin one. Similarly, on the upper part of the spectra, it can be seen that the magnitude of the strings' partials is higher in the rigid case compared to the thin one. Both these two effects contribute to substantially change the timbre of the tones. This is confirmed when listening to the simulated sound pressure.

3.3. Variations of hammer mass and velocity

In this section some properties resulting from changes in hammer mass and/or initial velocity are investigated. Such modifications have many consequences on piano tones. However, due to the lack of place, we limit ourselves to their effects in terms of acoustical efficiency. Figure 10 shows the evolution of the total energy of the sound (note C \sharp 5) for three different situations: the reference case, a hammer with normal velocity and mass divided by 2, and a hammer with normal mass whose initial velocity divided by 2. In contrary with the previous situations

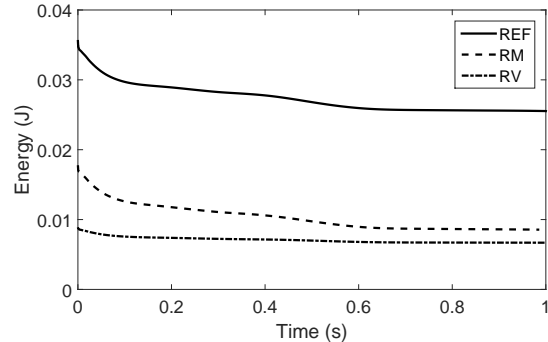


Figure 10: Temporal evolution of the total energy for the note C \sharp 5. Solid line: reference case (REF); dashed line: reduced hammer mass $M_H/2$ (RM); dash-dotted line: reduced initial velocity $V_H/2$ (RV).

(variations of string's tension and soundboard properties) the initial energy is different in the three cases, according to Eq. 1. While Figure 10 does not show salient effects, it is not the case

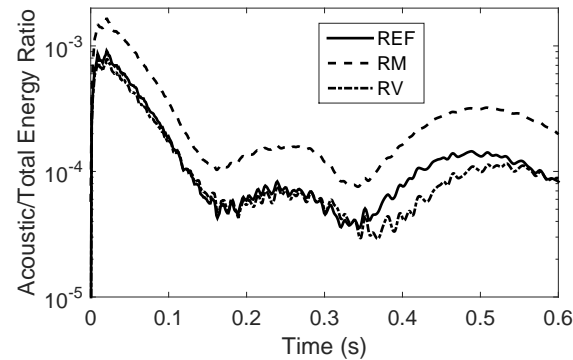


Figure 11: Relative acoustic energy. Solid line: reference case; dashed line: reduced hammer mass $M_H/2$; dash-dotted line: reduced initial velocity $V_H/2$.

for Figure 11 which shows the relative acoustic efficiency of the selected piano note in these three cases. Surprisingly, the hammer with reduced mass yields a significantly higher relative acoustic energy, whereas this relative energy only slightly depends on the hammer velocity. The relative soundboard energy (not shown here) shows similar features so that one has to seek upstream in the transmission chain of the piano, at the hammer-string level, for understanding this effect. In fact, as pointed out by the author in a previous study [2], reducing the hammer mass not only results in a decrease of the maximum hammer force, but also in a decrease in the hammer force duration, as seen in Figure 12. In contrast, reducing the hammer velocity induces almost only a reduction of force amplitude, with only a slight increase in the duration of the force pulse. As a consequence of pulse shortening, the slopes of the string's displacement increase. Since the force at the bridge is nearly proportional to the first spatial derivative of the displacement, it can be seen in Figure 13 that the bridge force pulses for the small hammer mass case have nearly the same amplitude as the reference one. In conclusion, this explains why both the soundboard and acoustic energy are comparable in these two cases. Finally, since the input energy is smaller in the case of reduced hammer mass, the soundboard and acoustic relative energy ratios are higher.

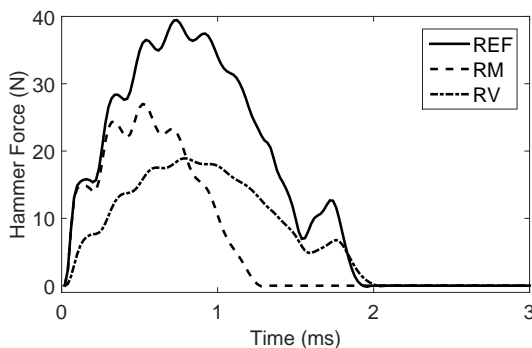


Figure 12: Hammer forces. Solid line: reference case; dashed line: reduced hammer mass $M_H/2$; dash-dotted line: reduced initial velocity $V_H/2$.

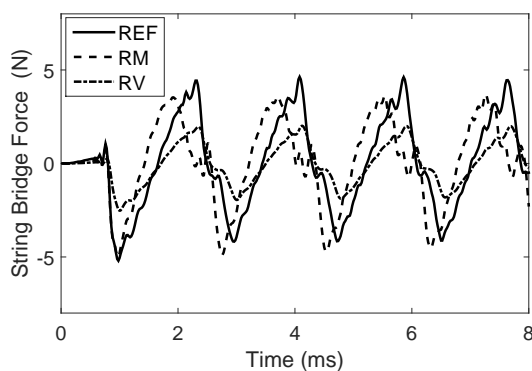


Figure 13: String forces at the bridge. Solid line: reference case; dashed line: reduced hammer mass $M_H/2$; dash-dotted line: reduced initial velocity $V_H/2$.

4. CONCLUSIONS AND FUTURE WORK

In this paper, the effects of structural changes related to hammers, strings and soundboard in a piano were analyzed in terms of energy. From the time evolution of acoustic, soundboard and total energies, it was shown how elementary modifications of structures affect the amplitude, decay time and spectral content of the sounds radiated by the piano. This analysis shed useful light on the energy transfer from strings to soundboard and air. One objective is to take advantage of these preliminary results to analyze real instruments in a historical perspective. It can be seen on historic pianos that several of the previously examined features coexist. Pianos built during the first half of the nineteenth century, for example, are characterized by reduced string tension, reduced hammer mass and thin soundboard, compared to modern pianos. One goal is then to measure and quantify the tonal differences between historic and modern instruments, and to relate them to intrinsic differences of structures. Another natural extension of this study is to use energy analysis for investigating refined aspects of piano manufacturing, such as the design of ribs and bridges, the choice of strings' material and the use of leather for the piano hammers.

The work presented in this paper was motivated by the interest to bring some light into the *global* energetic behavior of the piano. However, the *local*, or *note by note*, consequences of structural changes should not be forgotten. It has been seen, for example, that the eigenfrequencies of the soundboard increase with its rigidity. As a consequence, the soundboard mobility

will vary over a large frequency range significantly. This feature might induce some heterogeneities in the strings-soundboard coupling and, in turn, in the sound quality. The piano model used in this study is characterized by an accurate description of the losses, for each element (see the Appendix below). The modal approach used for the soundboard, in particular, allows a mode by mode adjustment of the damping. This feature should facilitate the simulation of soundboards made of different materials, and their comparisons in terms of tone quality. Finally, from a theoretical point of view, an important work remains to be done in order to determine to what extent the losses in strings and soundboard depend on their geometry, so that adjustments can be done in the model accordingly.

5. ACKNOWLEDGEMENTS

This project was supported by a Lise-Meitner-Fellowship of the Austrian Science Fund (FWF) [Project number M 1653-N30]. Numerical experiments presented in this paper were carried out using the PLAFRIM experimental testbed, being developed under the Inria PlaFRIM development action with support from LABRI and IMB and other entities: Conseil Régional d'Aquitaine, FeDER, Université de Bordeaux and CNRS (<https://plafrim.bordeaux.inria.fr/>).

6. APPENDIX: ENERGY LOSSES IN THE PIANO

This section summarizes, without demonstrations, the lossy terms used in the model for describing the dissipation phenomena in hammers, strings and soundboard. For simplicity, the expressions below are given in the case of a single string. The reader can refer to previous papers for details on the calculations, and for a more general formulation of the losses [1, 4].

6.1. Losses in a string

In order to account for frequency-dependent losses in a string in a convenient way, additional terms of the form:

$$r_u \frac{\partial u_s}{\partial t} - \eta_u \frac{\partial^3 u_s}{\partial t \partial x^2} \quad (11)$$

are added in the string equation [12]. The coefficients r_u and η_u are usually derived from experiments. Similar expressions are used for v_s and φ_s . As a consequence, one can show that the rate of energy loss for the transverse motion of the string is given by:

$$\frac{d}{dt} \mathcal{L}_u = r_u \int_0^L \dot{u}_s^2 dx + \eta_u \int_0^L \frac{d\dot{u}_s}{dx}^2 dx, \quad (12)$$

with analog expressions for v_s and φ_s . In total, the rate of energy in the string is given by:

$$\frac{d}{dt} \mathcal{E}_s = K_H \langle \dot{u}_s \rangle \Phi(\langle u_s \rangle(t) - \xi(t)) - \frac{d}{dt} \mathcal{L}_s \quad (13)$$

where the first term on the right-hand side accounts for the transfer of energy from hammer to string, and where the sum of energy losses in the string is of the form:

$$\mathcal{L}_s = \mathcal{L}_u + \mathcal{L}_v + \mathcal{L}_\varphi. \quad (14)$$

6.2. Losses in the hammer-string system

In order to account for the relaxation losses in the hammer felt, a dissipative term of the form

$$R_H \frac{d}{dt} \Phi (\langle u_s \rangle(t) - \xi(t)) \quad (15)$$

is added on the right-hand side of Eq. (5). Due to the action-reaction law, the energy gained by the string is now compensated by a decrease of hammer energy. As a consequence, taking further string and hammer losses into account, leads to the following energy rate for the isolated hammer-string system:

$$\frac{d}{dt} \mathcal{E}_{s,H} = -\frac{d}{dt} \mathcal{L}_s - \frac{d}{dt} \mathcal{L}_H \quad (16)$$

with $\frac{d}{dt} \mathcal{L}_H = R_H \Phi' (\langle u_s \rangle(t) - \xi(t)) [\dot{\langle u_s \rangle} - \dot{\xi}]^2$,

where \mathcal{L}_H is the energy loss in the hammer felt. When the hammer-string system is coupled to the soundboard at the bridge, an additional source of loss has to be considered for this system, as shown below.

6.3. Losses in the soundboard

In the present model, a modal approach is applied to the soundboard. The soundboard modes are calculated first, and the internal losses are assumed to be small enough so that each modal displacement q_n is described by a damped oscillator equation of the form:

$$m_n \ddot{q}_n + r_n \dot{q}_n + k_n q_n = f_n, \quad (17)$$

where f_n is the modal projection of the string force at the bridge. For each soundboard mode, the rate of energy is given by:

$$\frac{d}{dt} \mathcal{E}_{p,n} = f_n \dot{q}_n - r_n \dot{q}_n^2. \quad (18)$$

In total, since the modes are assumed to be decoupled, the rate of energy for the soundboard becomes:

$$\frac{d}{dt} \mathcal{E}_p = \sum_{n=1}^N f_n \dot{q}_n - \sum_{n=1}^N r_n \dot{q}_n^2 = \frac{d}{dt} \mathcal{E}_B - \frac{d}{dt} \mathcal{L}_p, \quad (19)$$

where \mathcal{E}_B is the coupling energy between the string and the soundboard at the bridge, and \mathcal{L}_p is the loss of energy in the soundboard. The energy of the soundboard is truncated to N modes ($N=800$ for the examples given in the present paper, see Fig. 6). To ensure the conservation of energy for the string-hammer-soundboard system, the rate $-\frac{d}{dt} \mathcal{E}_B$ has to be added in the right-hand side of Eq. (16). Finally, when the soundboard is coupled to the acoustic space, it is subjected to a loss rate of acoustic energy of the form $-\frac{d}{dt} \mathcal{E}_a$ to be added in the right-hand side of Eq. (19).

6.4. Decreasing energy for the complete piano

In summary, we can write the following balance of energy for all constitutive parts of the piano:

$$\begin{aligned} \frac{d}{dt} \mathcal{E}_{s,H} &= -\frac{d}{dt} \mathcal{L}_H - \frac{d}{dt} \mathcal{L}_s - \frac{d}{dt} \mathcal{E}_B, \\ \frac{d}{dt} \mathcal{E}_p &= \frac{d}{dt} \mathcal{E}_B - \frac{d}{dt} \mathcal{L}_p - \frac{d}{dt} \mathcal{E}_a. \end{aligned} \quad (20)$$

By summation, we find the total energy rate:

$$\begin{aligned} \frac{d}{dt} \mathcal{E}_{tot} &= \frac{d}{dt} (\mathcal{E}_{s,H} + \mathcal{E}_p + \mathcal{E}_a) \\ &= -\frac{d}{dt} (\mathcal{L}_s + \mathcal{L}_H + \mathcal{L}_p). \end{aligned} \quad (21)$$

Finally, through integration of Eq. (21), and considering further that the total energy is equal to \mathcal{E}_0 at the origin of time, while the lossy terms are equal to zero, we find:

$$\mathcal{E}_{tot}(t) = \mathcal{E}_0 - (\mathcal{L}_s + \mathcal{L}_H + \mathcal{L}_p)(t) = \mathcal{E}_0 - \mathcal{L}(t), \quad (22)$$

which corresponds to the energy curves shown in Figs. 3 and 10.

7. REFERENCES

- [1] J. Chabassier, A. Chaigne, and P. Joly, “Modeling and simulation of a grand piano,” *J. Acoust. Soc. Am.*, vol. 134, no. 1, pp. 648–665, 2013.
- [2] A. Chaigne and A. Askewfelt, “Numerical simulations of piano strings. II. Comparisons with measurements and systematic exploration of some hammer-string parameters,” *J. Acoust. Soc. Am.*, vol. 95, no. 3, pp. 1631–1640, 1994.
- [3] M. French, “Structural modifications of stringed instruments,” *Mech. Syst. and Signal Proc.*, vol. 21, pp. 98–107, 2007.
- [4] J. Chabassier, A. Chaigne, and P. Joly, “Time domain simulation of a piano. Part 1: model description,” *Mathematical Modelling and Numerical Analysis*, vol. 48, no. 5, pp. 1241–1278, 2014.
- [5] M. Novak Clinkscale, *Makers of the piano, 1700-1820*, Oxford University Press, Oxford, 1993.
- [6] M. Novak Clinkscale, *Makers of the piano, 1820-1860*, Clarendon Press, Oxford, 1999.
- [7] J. Chabassier and P. Joly, “Energy preserving schemes for nonlinear Hamiltonian systems of wave equations. Application to the vibrating piano string..,” *Comp. Meth. in Appl. Mech. and Eng.*, vol. 199, pp. 2779–2795, 2010.
- [8] X. Boutillon, “Model for piano hammers: Experimental determination and digital simulation,” *J. Acoust. Soc. Am.*, vol. 83, no. 2, pp. 746–754, 1988.
- [9] A. Stulov, “Experimental and computational studies of piano hammers,” *Acta Acustica united with Acustica*, vol. 91, no. 6, pp. 1086–1097, 2005.
- [10] J. P. D. Wilkinson, “Modal densities of certain shallow structural elements,” *J. Acoust. Soc. Am.*, vol. 43, no. 2, pp. 245–251, 1968.
- [11] F. Fahy, *Foundations of Engineering Acoustics*, Academic Press, London, 2000.
- [12] S. Bilbao, *Numerical sound synthesis. Finite differences schemes and simulation in musical acoustics.*, J. Wiley, Chichester, 2009.